

Electronic structure of small clusters of nickel and iron

Keeyung Lee,* Joseph Callaway, Kwok Kwong, Rongqi Tang, and Alfred Ziegler

Department of Physics and Astronomy, Louisiana State University, Baton Rouge, Louisiana 70803-4001

(Received 16 August 1984; revised manuscript received 26 October 1984)

We have performed self-consistent, spin-polarized calculations for free Fe_{13} , Ni_{13} , and Ni_{19} clusters with face-centered-cubic geometry and for a Fe_{14}C cluster with body-centered-cubic geometry. The calculations are made by expansion in a basis set of Gaussian orbitals. Results are discussed in relation to similar calculations for bulk metals. Comparison of the present results with our previous calculations for Fe_{15} shows that the d -level distribution in the nickel cluster is narrower in comparison with the bulk than was found for iron, but that the spin distribution is closer to the bulk. The central atom in the Fe_{13} cluster is strongly spin polarized oppositely to the surrounding atoms. Effects due to replacement of the central iron atom in Fe_{15} by carbon are studied. The ionization potential of Fe_{13} was found to be 5.41 eV.

I. INTRODUCTION

This work is a continuation of a previous calculation for small iron clusters in which results for the electronic structure of Fe_9 and Fe_{15} (in body-centered-cubic geometries)^{1,2} were presented. The most important findings of that work were (1) that the density of states for the Fe_{15} cluster approached rather closely that for bulk iron, (2) that the average magnetizations of both the Fe_9 and Fe_{15} clusters were considerably larger than that of the bulk, and (3) that the spin-density distribution for both clusters differed substantially from the bulk with a greater concentration of minority-spin density on the central atom. We found a greater resemblance between bulk and cluster (Fe_{15}) densities of states than reported in the discrete variational method (DVM) calculations of Guenzberger and Ellis.³

In the present paper we consider an Fe_{13} cluster in face-centered-cubic geometry; Ni_{13} and Ni_{19} clusters also with fcc geometry, and Fe_{14}C with bcc geometry. (The carbon atom replaces the central iron atom.) The results are compared with those obtained for the clusters we have studied previously and with the results obtained for some of these systems by other authors. Underlying this and similar work is the basic question: How rapidly (with respect to increasing number of atoms) does the electronic structure of an atomic cluster approach that of the bulk solid? It is of course, not possible to give definitive answers based on a small number of systems, but it appears from the calculations described here that the answer may be unexpectedly complex even when attention is focused on a restricted and particular subclass: that of ferromagnetic transition elements. The additional clusters considered in this work permit us to address the following specific questions: Does the good agreement between cluster and bulk energy-level distributions (densities of states) found for the case of Fe_{15} persist in the cases of other atoms and other geometries? Are the differences between cluster and bulk spin densities uncovered for Fe_{15} peculiar to iron or are similar results obtained for other transition metals? Although complete answers cannot be given here, the comparison of results for iron and nickel has proved to be very informative. In addition, it is our attention to investigate the electronic structure of dilute

alloys involving transition metals by means of fully self-consistent calculations for clusters containing one or more "impurity" atoms. The first of a projected series of calculations of this type is reported in this paper: Fe_{14}C , in which the central iron atom of the Fe_{15} cluster previously studied is replaced by a carbon atom. The bcc geometry considered here is, unfortunately, not the normal geometry for a carbon atom in iron. We hope to consider the more realistic interstitial geometry in a subsequent paper. However, some indications of the nature of impurity-produced electronic structure modifications can be obtained from the present work.

It must be emphasized that all calculations reported here pertain to free clusters. The problem of embedding the cluster so that it more nearly resembles a piece of the bulk metal is not considered here, but will, we anticipate, be addressed in future studies.

II. METHOD

These calculations employ the methods described in Refs. 1 and 2. Only the essential features will be mentioned here: The reader interested in details should consult the references cited. This work is based on density-functional theory in the local-spin-density approximation. An exchange-correlation potential parametrized by Rajagopal, Singhal, and Kimball is employed.⁴ The calculation is made by means of an expansion in Gaussian orbitals including 14 s -type functions, 9 p , and 5 d . The basis set is not contracted. The orbital exponents employed are those of Wachters,⁵ who reported Hartree-Fock calculations for free transition-metal atoms. When angular dependences are included, there are 66 independent functions per atom. However, use of the cubic symmetry of the clusters keeps the dimensions of the matrices which have to be diagonalized to manageable sizes.

Two additional characteristics of our procedures should be noted: (1) In order to avoid the calculation of enormous numbers of two-electron integrals, which increase as the fourth power of the number of Gaussians, we make an auxiliary fitting to the charge density⁶ using a separate, atom-centered, Gaussian orbital basis. A procedure was used in which the linear parameters of the fit are chosen

TABLE I. Comparison of properties of nickel clusters (energies in eV).

	Ni ₁₃ (This work)	Ni ₁₉ (This work)	Bulk Ni (Ref. 8)
$(n_{\uparrow} - n_{\downarrow})/N_A$	1.14	0.80	0.57
Occupied <i>s</i> -band width			
(↑)	8.1 ^a	8.7 ^a	9.0 ^b
(↓)	8.0 ^a	8.6 ^a	9.0 ^b
Occupied <i>d</i> -band width			
(↑)	4.3 ^c	4.8 ^d	4.5 ^e
(↓)	3.6 ^d	4.4 ^d	4.5 ^f
Total <i>d</i> -band width			
(↑)	4.3 ^g	4.8 ^h	4.5 ^e
(↓)	4.0 ⁱ	5.0 ^h	4.8 ^e
Range of exchange splitting (<i>d</i>)	0.3–1.3	0.2–1.0	0.31–0.63
Average exchange splitting (<i>d</i>)	0.85	0.61	
Exchange splitting (<i>sp</i>)	0.17 ^j	0.14 ^j	0.0

^a $\epsilon_F - 1a_{1g}$.^b $\epsilon_F - \Gamma_1$.^c $\epsilon_F - 1t_{2g}$.^d $\epsilon_F - 1e_g$.^e $X_5 - L_1$.^f $\epsilon_F - L_1$.^g $5e_g - 1t_{2g}$.^h $8t_{2g} - 1e_g$.ⁱ $5e_g - 1e_g$.^j $1a_{1g\uparrow} - 1a_{1g\downarrow}$.

variationally so as to produce minimum errors in the electrostatic energy of the electron distribution.⁷ (2) However, we were able to avoid the need to make a similar fit to the exchange-correlation potential. Matrix elements of this quantity were calculated by direct numerical integration using a special three-dimensional grid explicitly devised for this purpose.^{1,2}

III. RESULTS

A. Ni₁₃ and Ni₁₉

We will discuss first our results for the nickel clusters Ni₁₃ and Ni₁₉. These calculations were made assuming a central-atom–first-neighbor distance of 4.70 a.u., corresponding to bulk metallic nickel at $T=0$. Some characteristic numerical results are summarized in Table I, which includes values for bulk metallic nickel according to the band calculations of Ref. 8 for comparison. An energy-level diagram for Ni₁₃ is shown in Fig. 1 and for Ni₁₉ in Fig. 2.

In these calculations, we found that a pair of levels of opposite spins ($5e_{g\uparrow}, 5t_{2g\downarrow}$ for Ni₁₃ and $8t_{2g\uparrow}, 7e_{g\downarrow}$ for Ni₁₉) were very close together near the Fermi energy. Although these levels are not exactly degenerate, we considered them to be degenerate in our calculations in order to avoid oscillations in the iterative process leading to self-consistency. Electrons are assigned to these states in proportion to their degeneracy. This accounts for the fractional occupancy noted in Figs. 1 and 2.

Previously, two calculations for Ni₁₃ clusters by the $X\alpha$ scattered-wave method have been reported.^{9,10} The earlier of these⁹ obtained qualitatively very different level structures from that found in the present work. In particular the *d*-band width was roughly one-half that obtained here and the exchange splitting was also much smaller. A more recent calculation¹⁰ is only very sketchily reported without numerical data. However in this case also (on the

basis of graphical data) the *d* band seems to be more compressed with a different distribution of levels, but the exchange splitting seems to be in reasonable agreement with that found here. These are certainly differences in detail: We find the $6t_{2g\uparrow}$ level to be occupied whereas in Ref. 10, it is about 1 eV above the Fermi level (the position of $6t_{2g\uparrow}$ is essential to the argument of Ref. 10). The contact density at the nuclear sites are, in atomic units, -0.348 for the central atom and 0.107 for the outer shell.

We will discuss here principally the results for Ni₁₉.

An integrated density of states (number of levels per atom with energy less than or equal to E) can be defined for the cluster and compared with corresponding results for the bulk metal. This comparison contains no arbitrary level broadening. It is, however, convenient to adjust the

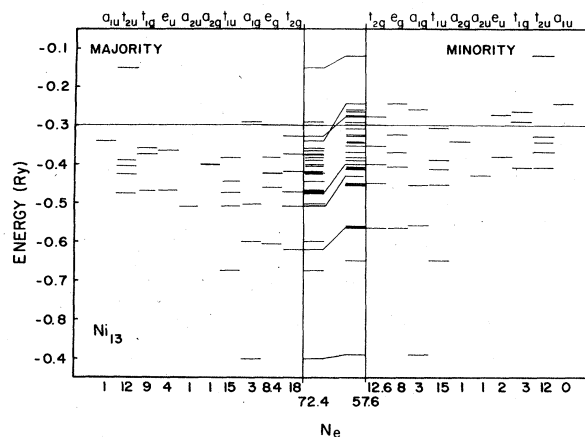
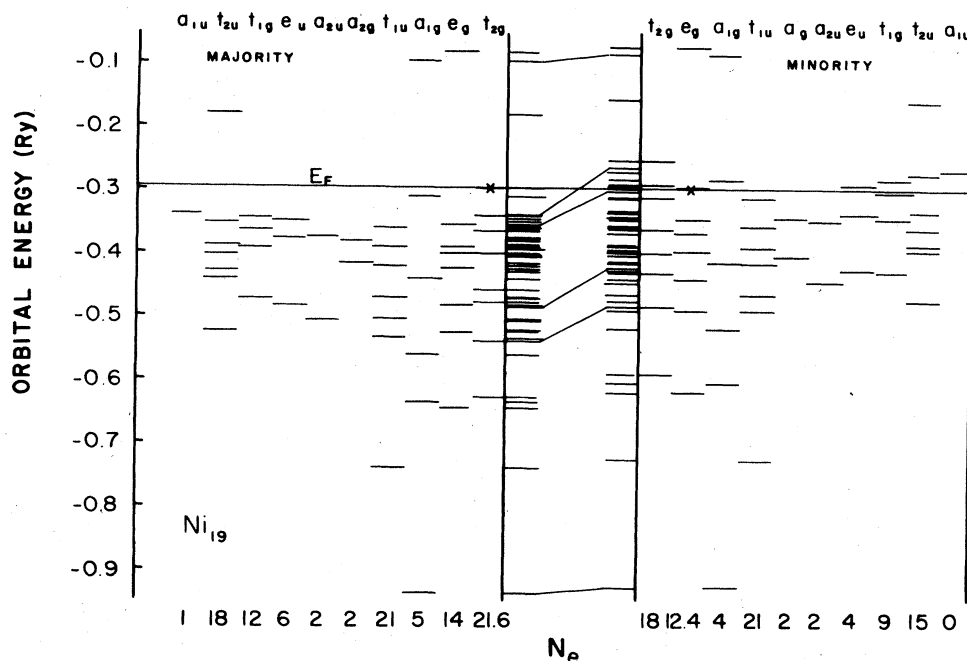


FIG. 1. Energy-level diagram for the Ni₁₃ cluster. The symmetries of levels and the occupancies (N_e) are given. The solid vertical line in the figure shows the position of the Fermi level, and the crosses indicate the position of levels at the Fermi energy (see text for comments regarding fractional occupancy).

FIG. 2. Energy-level diagram for the Ni_{19} cluster.

energy scales so that the Fermi energies coincide. The integrated densities of states for Ni_{19} is shown and compared with that for the metal in Fig. 3 (both spins) and for majority and minority spins separately in Fig. 4. The integrated densities are of particular interest because no arbitrary level broadening is involved.

Although the overall d -band width as determined from

states at the top and bottom of the distribution agrees well with the solid results, it is apparent from Fig. 3 that the bulk of the d -level distribution is somewhat narrower in the cluster than in the solid. (We refer to the level distribution in the cluster as a band although it is, of course, not continuous). If the d -band width is estimated roughly from Fig. 3, we obtain an estimate of about 3.4 eV, which, perhaps accidentally, is closer to the experimental results for the d -band widths in nickel metal¹¹ than are the values obtained from the band calculations for the metal. This

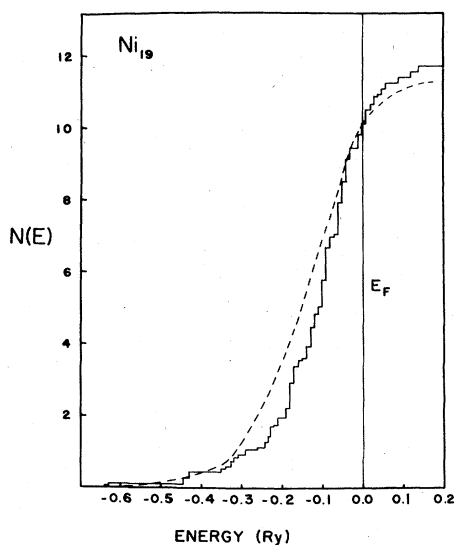


FIG. 3. Integrated density of states per atom for Ni_{19} (including both spins). The ordinate shows the number of states per atom. Results from the band calculation of Ref. 8 for the corresponding quantity for bulk metallic nickel are shown by a dashed line. The zero of energy has been shifted in each case so that the Fermi levels coincide at $E=0$.

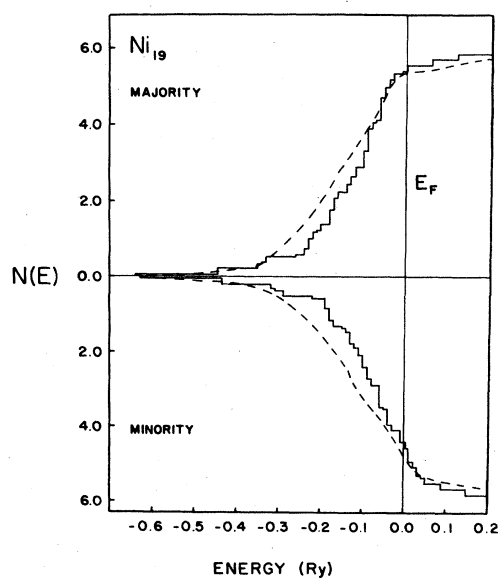


FIG. 4. Integrated density of states for Ni_{19} with majority and minority spins separated.

result, however, probably lacks fundamental significance. The discrepancy between calculated cluster and bulk bandwidths is noticeably larger for Ni_{19} than for Fe_{15} (according to our previous calculations).

On the other hand, the magnetic moment of the Ni_{19} cluster is considerably closer to the bulk value (both absolutely, and relative to the difference in moment between free atom and bulk) than was found previously for Fe_{15} . This may be in part a geometrical effect: We find for the Fe_{13} cluster with fcc geometry (discussed in more detail below) a smaller moment than for Fe_{15} . Typical d -level exchange splittings in Ni_{19} are not very different for those calculated for bulk nickel, and are larger than the experimental results for the metal.

The most obvious characteristic of the d -level distribution in the Ni_{19} cluster (see Fig. 2) is that the majority-spin d levels are almost completely full, while there is a tail of the minority-spin d band extending a short distance in energy above E_F . This is also true for the bulk metal. Examination of Figs. 4 and 5 shows that the proportion of states extending above E_F is similar to the bulk for both spins. In order to make a more detailed comparison, we constructed a cluster density of state (CDOS) by replacing the sharp levels actually calculated by Gaussian of a common width 0.2 eV. This choice of width, although arbitrary, was found in Ref. 1 to give a CDOS for Fe_{15} which had a very pleasing resemblance to the bulk density of states, although an even better resemblance could be obtained if the predominately s - p levels are broadened more than the d levels. The CDOS constructed for Ni_{19} are shown in Fig. 5 (both spins) and Fig. 6 (separate spins), where the cluster results are compared with those from the band calculation of Ref. 8.

There is for Ni_{19} , as for the previously studied Fe_{15} , a substantial degree of general qualitative agreement between cluster and bulk results. This is particularly striking for the minority-spin distribution in the neighborhood of E_F . For both spins, the average s - p densities (states

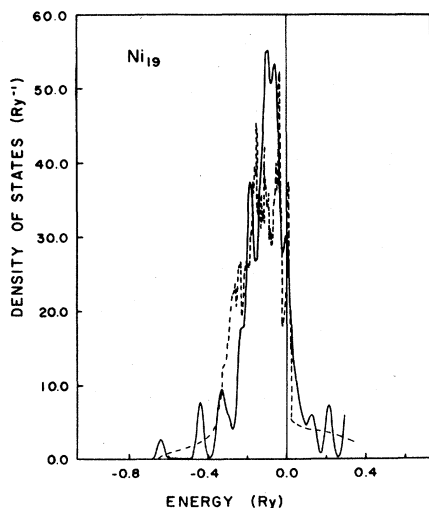


FIG. 5. The cluster density of states per atom for Ni_{19} including both spins. Solid line, present calculation; dashed line band-calculation results (Ref. 8).

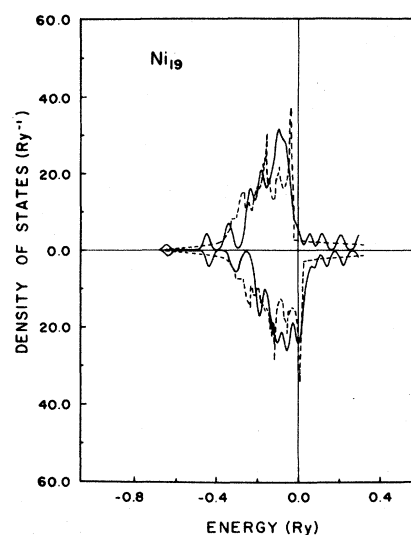


FIG. 6. Density of states (separate spins) for Ni_{19} . Solid line, present calculation; dashed line, band calculation.

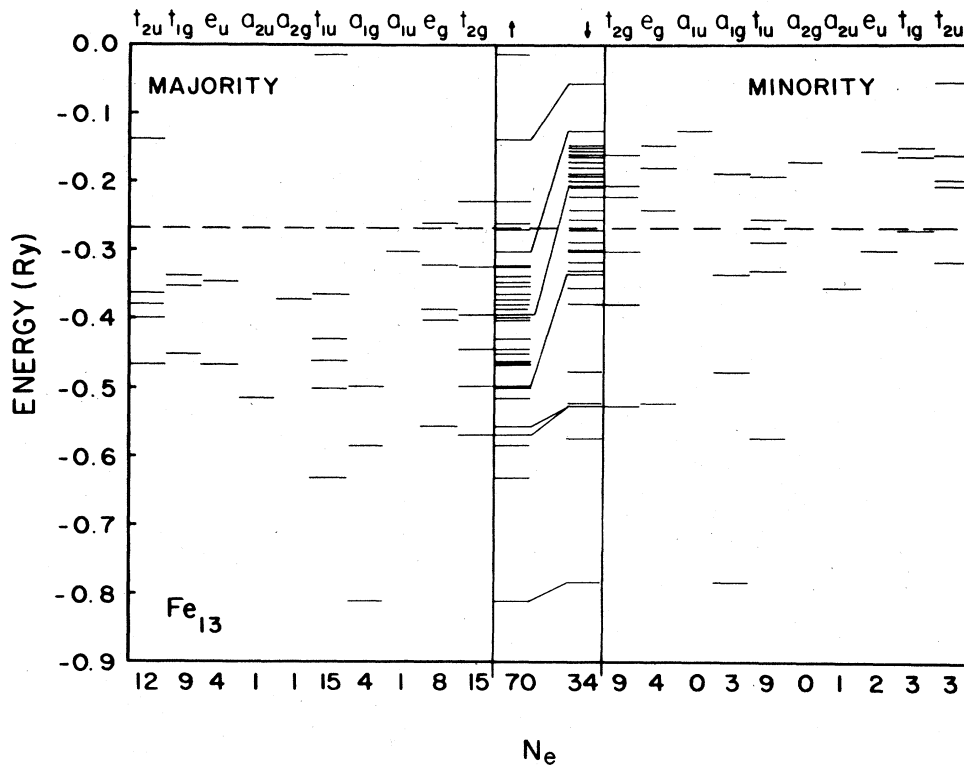
above and below the d -level complex) seems to be in about the correct ratio in comparison to the d -state densities. The sharp structure of the solid density of state is, of course, missing in the cluster as a result of our definition of the CDOS. There is a relatively broad peak with a shoulder in the majority-spin CDOS just below E_F in contrast to the narrow, high peak found for the solid. In addition, the CDOS is depleted, relative to the solid, near the bottom of the d complex and enhanced near the top: another manifestation of the general band narrowing mentioned above.

The contact spin densities at the nuclear sites are, in atomic units, -0.091 (central atom), -0.106 (first neighbors), and -0.235 (second neighbors). For comparison, the value obtained in Ref. 8 in the case of bulk metallic nickel was -0.110 . The agreement between the central-atom contact spin density and that of the bulk is much improved for the larger Ni_{19} cluster compared to the Ni_{13} cluster, and also much better than was found in the case of the Fe_9 and Fe_{15} clusters previously studied.

In contrast to Fe_{15} , we do not find a minority-spin-dominated central atom. In the former case, the core levels of the central atom, $1s$ - $3p$ had a slight negative-spin polarization (see further discussion below). This is absent in Ni_{19} : All the central-atom core levels have a conventional polarization with those of \uparrow spin lower in energy than those of \downarrow spin. There is some charge flow from the central atom to its neighbors, and the region of majority spin on the central atom is surrounded by an interstitial region in which there is a slight excess of minority-spin electrons.

B. Fe_{13}

We decided to investigate Fe_{13} to see whether our results for a minority-spin-dominated central atom would also occur in fcc geometry. Bulk fcc iron, if it existed at $T=0$ K, would probably be antiferromagnetic.¹² Levels

FIG. 7. Energy-level diagram for Fe_{13} .

of the Fe_{13} cluster were calculated assuming that the distance between the central atom and the first neighbors was 4.81 a.u. corresponding to a fcc structure with $a=6.80$ a.u., which is the lattice constant which gives a volume per atom (in bulk iron) equal to that of normal bcc iron.

An energy-level diagram for Fe_{13} is shown in Fig. 7. Some numerical results appear in Table II which also contains, for comparison, our previous results for Fe_9 , Fe_{15} , and for bulk iron.¹³ Bandwidth definitions for the bcc

systems are given in Ref. 1. The definitions used for the fcc case are similar. A very brief report (without numerical data) of an $X\alpha$ scattered-wave calculation for Fe_{13} may be found in Ref. 10. It will be seen from Table II that the bandwidths for Fe_{13} are intermediate between those for Fe_9 and Fe_{15} but the magnetic moment per atom, and the exchange splitting are slightly smaller. We do find that the central atom is minority-spin dominated. Core-level energies for the central atom and first neighbor are given in Table III, where results for Fe_{15} are also

TABLE II. Comparison of properties of iron clusters (energies in eV).

	Fe_9 (Ref. 1)	Fe_{13} (Present)	Fe_{15} (Ref. 1)	Fe_{14}C (This work)	Bulk Fe (Ref. 13)
$(n_\uparrow - n_\downarrow)/N_A$	2.89	2.77	2.93	3.07	2.16
Occupied <i>s</i> -band width					
(\uparrow)	6.7	7.4 ^a	7.7	6.2 ^b	8.20
(\downarrow)	6.3	7.0 ^a	7.2	5.5 ^b	8.03
Occupied <i>d</i> -band width					
(\uparrow)	3.8	4.1 ^c	4.4	3.3 ^d 3.9 ^c	4.75
(\downarrow)	2.8	3.5 ^c	3.3	1.9 ^e 2.2 ^c	3.60
Total <i>d</i> -band width					
(\uparrow)	4.4	4.5 ^f	4.7	3.3 ^d	5.13
(\downarrow)	4.0	5.2 ^g	5.3	3.7 ^d	6.12
Range of exchange splitting (<i>d</i>)	0.7–3.1	1.1–2.7	1.0–2.7	1.5–2.9	1.1–2.2
Average exchange splitting (<i>d</i>)	2.3	2.0	2.4	2.4	
Exchange splitting (<i>sp</i>)	0.4	0.4	0.5	0.5–1.1	0.16–0.85

^a E_F-1a_g .^b E_F-1t_{1u} .^c E_F-1t_{2g} .^d $6t_{2g}-1t_{2g}$.^e $3\epsilon_{1g}-1t_{2g}$.^f $6t_{2g}-1t_{2g}$.^g $5e_g-1t_{2g}$.

TABLE III. Core-level energies (Ry) for the central and first-neighbor atoms. In the latter case there are slight differences which depend on symmetry. The values quoted are from the a_{2u} representation for Fe_{15} and the e_g (s states) and a_{2u} (p states) for Fe_{13} .

	Central atom		First neighbor	
	Fe_{13}	Fe_{15}	Fe_{13}	Fe_{15}
$1s_{\uparrow}$	-507.846	-507.886	-507.795	-507.850
$1s_{\downarrow}$	-507.847	-507.886	-507.794	-507.848
$2s_{\uparrow}$	-58.745	-58.809	-58.760	-58.817
$2s_{\downarrow}$	-58.801	-58.813	-58.650	-58.710
$2p_{\uparrow}$	-50.723	-50.776	-50.729	-50.770
$2p_{\downarrow}$	-50.765	-50.778	-50.634	-50.684
$3s_{\uparrow}$	-6.392	-6.454	-6.507	-6.531
$3s_{\downarrow}$	-6.503	-6.464	-6.287	-6.318
$3p_{\uparrow}$	-4.058	-4.120	-4.183	-4.194
$3p_{\downarrow}$	-4.167	-4.132	-3.978	-3.974

presented for comparison. Note that the central-atom core levels are negatively polarized; that is, that the \downarrow spin states on this atom are lower in energy than those of \uparrow spin. The negative polarization is larger for Fe_{13} than for Fe_{15} .

In contrast, all the core levels obtained in the bulk-metal band-structure calculation of Ref. 13 show the conventional spin polarization (majority-spin levels lower in energy than minority). This is obtained even though the band calculations reveal the expected negative hyperfine fields at the nuclear sites (both in iron and nickel). The exchange splitting of the core levels need not be rigorously proportional to the site magnetic moment, but the core levels sample the local magnetization density in relatively well-defined regions of space; that is, in the region in which electrons of the particular shell considered dominate the charge density.

A rough numerical integration (rough because the definition of the limits is somewhat arbitrary), suggests the central atom has about 1.7 more electrons of minority spin (\downarrow) than of majority spin. A minority-spin excess on the central atom was also found for the Fe_{15} cluster, but is much larger in the present case.

The spatial distribution of the spin densities may perhaps be rationalized in the following way: The exchange-correlation potential is attractive but relative to the local average, electrons whose spin direction corresponds to that of the local majority experience attraction, while if the spin is parallel to the local minority the interaction is repulsive. Hence there is a tendency for the spin densities to separate spatially. We might at first expect that the minority-spin electrons would be pushed toward the outside of the cluster. In the bulk metals there is a tendency for minority-spin electrons to be pushed toward the boundaries of the atomic cell. However, in the free cluster the potential rises rapidly toward the vacuum level beyond the last shell of atoms, and it becomes energetically unfavorable for electrons to move toward the outside. The result appears to be that the minority spins move preferentially into the center of the cluster where they become the local majority. Since the relative repulsion experienced by minority spins is roughly proportional to the local magnetization density, the tendency toward

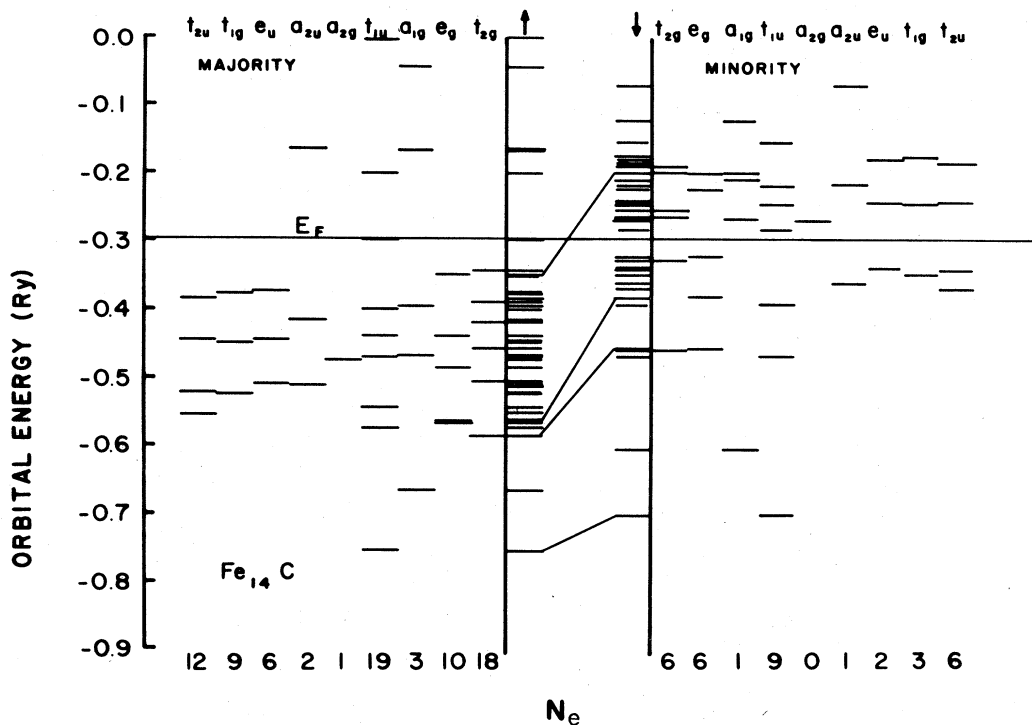
spatial separation would be expected to be more pronounced for iron (on account of the larger atomic moment) than for nickel, and more pronounced for the close-packed fcc geometry than for bcc. The contact spin densities at the nuclear sites are -0.02 a.u. for the central atom and -0.32 for the first neighbors.

Since there is some experimental information concerning ionization potentials of small free-iron clusters,¹⁴ we performed a transition-state¹⁵ calculation for Fe_{13} . Our result is 5.41 eV even for this quantity. The experimental value is in the range 5.6–6.4 eV.¹⁴ We think the agreement is reasonable in view of the fact that the geometry of the experimental cluster is unknown. The calculated ionization potential of Fe_{13} is slightly larger than for Fe_9 (5.2 eV), which agrees with the experimental observation that the ionization potential is larger for iron clusters with 13 to 19 atoms than for those with 9 to 12 atoms.¹⁴

C. Fe_{14}C

The energy levels for this cluster are shown in Fig. 8 and numerical data is included in Table II. The $2s$ levels of the carbon atom are not shown in the diagram. They are well separated from the other levels [lying at energies of -1.14 Ry (\uparrow) and -1.12 Ry (\downarrow)], and appear not to mix strongly with any of the levels of the iron neighbors. The spin polarization is in the same direction for the carbon $1s$ level, indicating that the carbon atom is slightly spin polarized in the conventional way: Levels with spin parallel to the Fe neighbors are slightly lower in energy.

On the other hand, the $2p$ levels of the carbon appear to have mixed strongly with the $4s$ and $3d$ functions of the iron neighbors. The net result is that there is one additional $t_{1u\uparrow}$ (partially) occupied state (which defines the Fermi level) for Fe_{14}C in comparison with Fe_{15} . Since there are no $3d$ functions on the central atom, the number of available $3d$ states is reduced, and so is the width of the d -level complex we call the d band. Comparison of the CDOS for Fe_{14}C with that for Fe_{15} shows close agreement near the top of the d -level complex, but disagreement near the bottom. Fe_{14}C lacks some of the low-lying s and d levels of Fe_{15} . The replaced central atom of Fe_{15} had contributed substantially to these levels. (This will also be ap-

FIG. 8. Energy-level diagram for Fe_{14}C .

parent from comparison of Fig. 8 of this paper with Fig. 2 of Ref. 1.) Therefore, in the possibly hypothetical case of a substitutional carbon atom in bulk iron, the principal effect on the density of states should be a depletion near the bottom of the s - d band.

A contour map of the charge density in the (100) plane is shown in Fig. 9. The existence of directional bonds between the iron and carbon atoms is clearly indicated. By

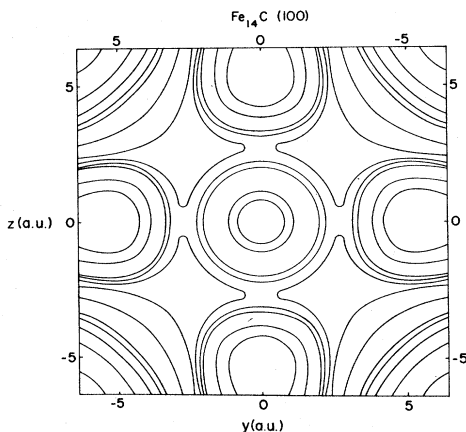


FIG. 9. Contours of constant charge density in the (100) plane for Fe_{14}C . The carbon atom is at the center of the figure and the centers of the iron atoms are just slightly inward from the 0 tic marks on the axes. The outermost (connected) contour around each atom corresponds to a charge density of 0.03 in atomic units; the next two inwards correspond to 0.04 and 0.05; the two innermost contours correspond to 0.2 and 0.8. The contours in the corners correspond to (from the corners inwards) 0.002, 0.003, 0.004, 0.005, 0.010, and 0.020.

numerical integration, we estimate that the net moment on the carbon atom is about $0.08\mu_B$. The contact spin density at the carbon site is 0.40 in atomic units, -0.07 at the first-neighbor iron sites, and -0.45 on the outer iron shell.

IV. CONCLUSIONS

We have completed self-consistent spin-polarized calculations for free Fe_{13} , Ni_{13} , Ni_{19} , and Fe_{14}C clusters using the local-spin-density approximation to density-functional theory. Our results for these clusters have been compared with our previous calculations for Fe_9 and Fe_{15} clusters. The most general conclusion of this work is that, although there is a substantial resemblance between a suitably defined free-cluster density of states and that of the bulk metal for clusters of the general range of sizes considered here, the magnetic properties may differ substantially from those of the bulk. The degree of departure from bulk properties depends on the type of atom and the geometrical arrangement. Specifically, in contrast to the Fe_9 and Fe_{15} clusters studied in previous work, the nickel clusters, which have fcc geometry, show magnetic moments (and spin-density distributions) that are closer to those of the bulk metal. However, d -level distribution in the nickel clusters is somewhat more compressed in energy, in comparison with the bulk metal than was found for Fe_9 and Fe_{15} .

In regard to band widths, Fe_{13} generally interpolates smoothly between Fe_9 and Fe_{15} even though the atomic arrangement is different. It does differ in having a smaller net magnetic moment than the bcc geometry clusters. The central atom has a substantial excess of electrons of

minority spin while there is only small minority-spin excess in Fe_9 and Fe_5 . The differences between Fe_9 , Fe_{13} , and Fe_{15} therefore indicate the existence of geometric effects in the spin density not immediately related to cluster size. This type of spin distribution was not found for the nickel clusters studied, in which the central atom is conventionally spin polarized (majority spin).

The results for the Fe_{14}C cluster show bonding between the central carbon and surrounding iron atoms. The car-

bon atom is weakly spin polarized by the surrounding iron atoms.

ACKNOWLEDGMENT

This work was supported in part by the U.S. Army Research Office under Contract No. DAAG29-K-81-8006.

*Present address: Argonne National Laboratories, Argonne, IL 60439.

¹K. Lee, J. Callaway, and S. Dhar, *Phys. Rev. B* **30**, 1724 (1984).

²K. Lee, Ph.D. thesis, Louisiana State University, Baton Rouge, 1984 (unpublished), available from University Microfilms International, Ann Arbor, Michigan, 48106.

³D. Guenzberger and D. E. Ellis (unpublished).

⁴A. K. Rajagopal, S. P. Singhal, and J. Kimball (unpublished), as quoted by A. K. Rajagopal, in *Advances in Chemical Physics*, edited by G. I. Prigogine and S. A. Rice (Wiley, New York, 1979), Vol. 41, p. 59.

⁵A. J. H. Wachters, *J. Chem. Phys.* **52**, 1033 (1970).

⁶H. Sambe and R. H. Felton, *J. Chem. Phys.* **62**, 1122 (1975).

⁷J. W. Mintmire and B. W. Dunlap, *Phys. Rev. A* **25**, 88 (1983).

⁸C. S. Wang and J. Callaway, *Phys. Rev. B* **15**, 298 (1977), J. Callaway, in *Physics of Transition Metals, 1980*, edited by P. Rhodes (IOP, London, 1981), p. 1.

⁹R. P. Messmer, S. K. Knudson, K. H. Johnson, J. B. Diamond, and C. Y. Yang, *Phys. Rev. B* **13**, 1396 (1976).

¹⁰J. Kaspar and D. R. Salahub, *Phys. Rev. Lett.* **47**, 54 (1981).

¹¹F. A. Himpfel, J. A. Knapp, and D. E. Eastman, *Phys. Rev. B* **19**, 2919 (1979); W. Eberhardt and E. W. Plummer, *ibid.* **21**, 3245 (1980).

¹²J. Kubler, *Phys. Lett.* **81A**, 81 (1981).

¹³J. Callaway and C. S. Wang, *Phys. Rev. B* **16**, 2095 (1977).

¹⁴E. A. Rohlfing, D. M. Cox, and A. Kaldor, *Chem. Phys. Lett.* **99**, 161 (1983).

¹⁵J. C. Slater, *The Self Consistent Field for Molecules and Solids* (McGraw-Hill, New York, 1974).